Supporting Information

Visible-light-driven valorization of 5-hydroxymethylfurfural over a hollow Co_3O_4@$Zn_3In_2S_6$ nanocage in base-free water and air atmosphere

Rong Dang[a], Kexin Fan[a], Yan-Ning Wang[b], Guangsheng Zhu[a], Liu Liu[c], Zifu Hu[a], Taolian Guo[*a], Wu Chen[*a], Fengxiang Chen[*a]

[a]National Local Joint Engineering Laboratory for Advanced Textile Processing and Clean Production, and State Key Laboratory of New Textile Materials and Advanced Processing, Wuhan Textile University, Wuhan 430200, China

[b]College of Chemistry and Chemical Engineering, Xinyang Normal University, Xinyang, Henan 464000, China

[c]Analytical and Testing Center, Wuhan Textile University, Wuhan 430200, China

*Corresponding authors.

E-mail addresses: tlguo@wtu.edu.cn (T. Guo); wuchen@wtu.edu.cn (W. Chen); fxchen_czx@wtu.edu.cn (F. Chen)

Experimental section

Materials. All solvents and reagents were purchased from commercial sources and used without further purification., Methanol (AR), ethanol (AR), acetonitrile (HPLC), sopropanol were purchased from Sinopharm Chemical Reagent Co., Ltd. 2-Methylimidazole, $InCl_3 \cdot 4H_2O$, $ZnSO_4 \cdot 7H_2O$, Co $(NO_3)_2 \cdot 6H_2O$, thioacetamide (TAA), cetyltrimethylammonium bromide (CTAB), 6-di-tert-butyl-4-methylphenol (BHT), HMF, DFF, FFCA, HMFCA and other chemicals involved in this work were purchased from Aladdin Reagent Co., Ltd. (Shanghai, China).

Synthesis of ZIF-67. ZIF-67 was synthesized using a solvothermal method, building upon previous research.[1] Initially, 3.0 g of 2-methylimidazole ($C_4H_6N_2$) and 1.5 g of Co $(NO_3)_2 \cdot 6H_2O$ were combined in 40 mL of methanol (CH_3OH) and subjected to sonication for 10 minutes. Subsequently, the 2-methylimidazole solution was incorporated into the Co $(NO_3)_2 \cdot 6H_2O$ solution, and the resulting mixture was stirred for 24 hours at ambient temperature. After stirring, the mixture underwent centrifugation, leading to the formation of ZIF-67.

Synthesis of hollow Co_3O_4. Firstly, the ZIF-67 precursor was synthesized through a solvothermal method according to the reported research.[1] And then, the synthesized ZIF-67 was calcined in air atmosphere at 450 °C with a heating rate of 2 °C/min, and kept at 450 °C for 2 h to yield hollow Co_3O_4.

Synthesis of $Zn_3In_2S_6$. Firstly, 3 mmol of $ZnSO_4 \cdot 7H_2O$, 2 mmol of $InCl_3 \cdot 4H_2O$, and 6 mmol of thioacetamide (TAA) were was uniformly dispersed in 35 mL of deionized water and stirred for 20 min. Then, 0.32 g of cetyltrimethylammonium bromide (CTAB) was introduced gradually under stirring, keeping stirring for an additional 30 min. Finally, the mixture was transferred into a 50 mL Teflon-lined stainless-steel autoclave and maintained at 160 °C for 12 h. The resulting precipitate was collected undergoing centrifugation, washing and drying.

Synthesis of ZC-x. The ZC-*x* composites were synthesized by *in situ* growing method. Initially, a specified amount of Co_3O_4 was uniformly dispersed in 35 mL of deionized water and stirred for 20 min. Then, 3 mmol of $ZnSO_4 \cdot 7H_2O$, 2 mmol of $InCl_3 \cdot 4H_2O$, and 6 mmol of thioacetamide (TAA) were sequentially added to the solution. Subsequently, 0.32 g of cetyltrimethylammonium bromide (CTAB) was introduced gradually under stirring, keeping stirring for an additional 30 min. Finally, the mixture was transferred into a 50 mL Teflon-lined stainless steel autoclave and maintained at 160 °C for 12 h. The resulting precipitate was collected undergoing centrifugation, washing and drying. The synthesized samples were denoted as ZC-*x*, where *x* represent the percentage of Co_3O_4 in the heterojunction.

Characterizations. The crystalline structure of as-synthesized samples was characterized by an X-ray diffractometer (XRD, Bruker D8 Advance, Germany) using Cu Kα radiation (40 KV, 40 mA). The Ultraviolet-visible diffuse reflectance spectra (UV-vis DRS) were obtained by Shimadzu UV-2600. The morphology and microstructure of the samples were observed using a field-emission scanning electron microscope (SEM, Crossbeam 350, Zeiss) and a transmission electron microscope (TEM, FEI Tecnai G2 F30). X-ray photoelectron spectroscopy (XPS) spectra were recorded using Escalab 250Xi instrument (Thermo Scientific) equipped with an Al Kα microfocused X-ray source. The porosity structure and specific surface area were studied by nitrogen adsorption-desorption measurements using an Autosorb IQ Chemisorption/Physisorption Analyzer (ASAP 2460-4MP). The steady-state photoluminescence (PL) spectra and time-resolved photoluminescence (TRPL) decay plots were detected by the spectrophotometer with an excitation wavelength of 375 nm.

Photocatalytic performance evaluation. The photocatalytic oxidation of HMF was conducted in a

custom-designed multichannel photoreactor equipped with a 24 W Blue LED lamp. In detail, 20 mg of catalyst was dispersed into 5 mL of HMF solution (5 mM in deionized water) in a 10 mL quartz tube and then underwent ultrasonication for 10 min in air atmosphere, followed by stirring under irradiation for 3 h. The entire reaction process was carried out at room temperature. The product analysis was performed by an Agilent 1220 infinity HPLC instrument equipped HC-C18 column.

Product analysis. To quantify the product, a syringe was used to collect 1 mL of the reaction solution, which was subsequently filtered through a 0.22 μm PVDF membrane. An Agilent 1220 Infinity HPLC instrument was employed for the analysis of the product. An Agilent HC-C18 column was utilized to achieve the successive separation of furan compounds, namely HMF, DFF, FFCA, and FDCA. These compounds were identified using a UV detector operating at 254 nm. The mobile phase comprised a 5 mM ammonium formate solution mixed with acetonitrile at a 9:1 v/v ratio, and the flow rate was adjusted to 1.0 mL min^{-1}. The temperature of the column oven was held steady at 25 °C. The retention durations recorded for FDCA, HMFCA, FFCA, HMF, and DFF were 2.5, 3.0, 3.5, 6.6, and 8.2 minutes, respectively.

The conversion of HMF, yield and selectivity of products are calculated using the following equations:

$$HMF\ conversion\ (\%) = \frac{c(HMF)_{in} - c(HMF)_{out}}{c(HMF)_{in}} \times 100\%$$

$$DFF\ selectivity\ (\%) = \frac{c(DFF)_{out}}{c(DFF)_{out} + c(FFCA)_{out}} \times 100\%$$

$$DFF\ yield\ (\%) = \frac{c(DFF)_{out}}{c(HMF)_{in}} \times 100\%$$

where c $(HMF)_{in}$ is the initial reaction concentration of HMF; c $(HMF)_{out}$, c $(DFF)_{out}$ and c $(FFCA)_{out}$

are the ending reaction concentration of HMF, DFF and FFCA, respectively.

Quantitative experiment of $\cdot O_2^-$. The concentration of superoxide radicals ($\cdot O_2^-$) was determined using nitro blue tetrazolium (NBT) as a selective scavenger, which reacts with $\cdot O_2^-$ to produce water-insoluble purple formazan. Experiments were conducted under visible light ($\lambda \geq 400$ nm) in air-saturated aqueous environment. In a typical procedure, 5 mg of catalyst was dispersed in 20 mL of an NBT aqueous solution (40 mg/L). The mixture was first stirred in the dark for 30 min to establish adsorption–desorption equilibrium. During irradiation, aliquots were collected at specified time intervals, followed by filtration to remove the photocatalyst. The $\cdot O_2^-$ concentration was quantified based on the degradation of NBT, monitored by the decrease in absorbance at 259 nm.

Photoelectrochemical measurements. The photoelectrochemical properties were measured using a workstation (CHI660E). The FTO substrates coated with samples were employed as the working electrodes. The working electrode area was 1 cm^2 with 0.5 M Na_2SO_4 solution as electrolyte. The Pt and Ag/AgCl electrodes were used as counter and reference electrodes, respectively. The Pt and Ag/AgCl electrodes were served as counter and reference electrodes, respectively. Photocurrent experiments were performed under Xe lamp. Mott Schottky plots were measured at alternating current (AC) frequencies of 500 Hz and 1000 Hz.

Theoretical calculations. Density function theory (DFT) calculations were performed by using the CP2K-2023.2 package. Perdew-Burke-Ernzerh (PBE) of functional was used to describe the system.[2] Unrestricted Kohn-Sham DFT has been used as the electronic structure method in the framework of the Gaussian and plane waves (GPW) way. The Goedecker-Teter-Hutter (GTH) pseudopotentials and Double-ζ molecularly optimized basis sets (DZVP-MOLOPT-GTH) have been used for all elements.

The Brillouin zone was sampled with gamma points for surface calculation. A plane-wave energy cutoff of 400 Ry (1Ry = 13.606 eV) has been employed. The geometries were optimized using the Broyden-Fletcher-Goldfarb-Shanno (BFGS) algorithm. The convergence threshold of density matrix during self-consistent field (SCF) method was $1*10^{-5}$ Hartree, and convergence criterion for the forces was set to $4.5*10^{-4}$ Bohr/Hartree. A vacuum layer of 15 Å was constructed to eliminate interactions between periodic structures of surface models. The van der Waals (vdW) interaction was amended by the DFT-D3 method of Grimme.

Supplementary Figures and Tables

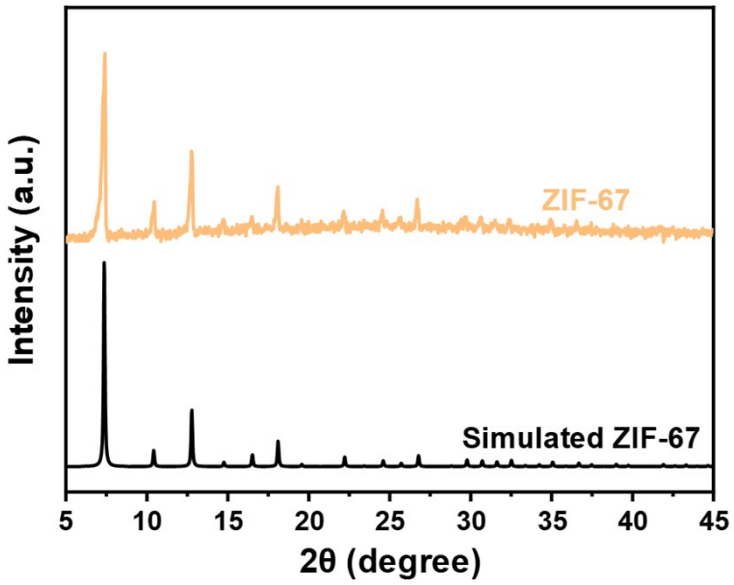

Fig. S1 XRD patterns of ZIF-67 and simulated ZIF-67.

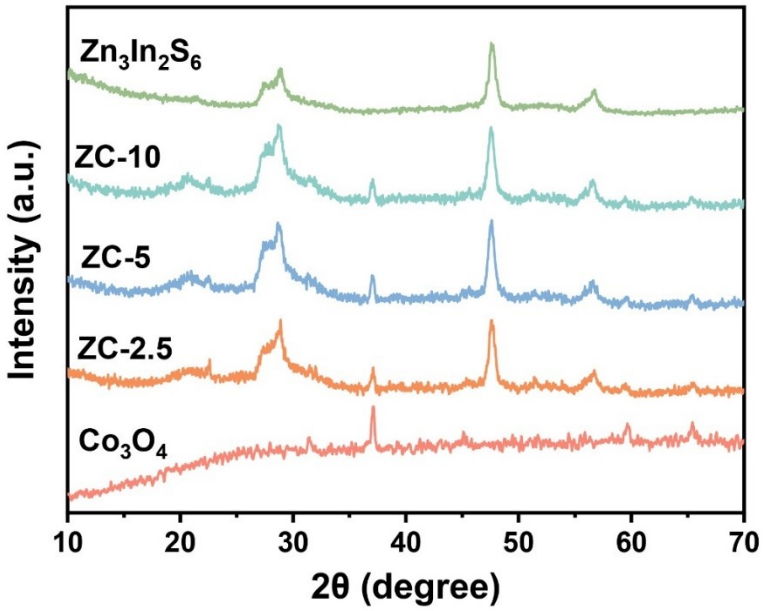

Fig. S2 XRD patterns of Co_3O_4, $Zn_3In_2S_6$, and ZC.

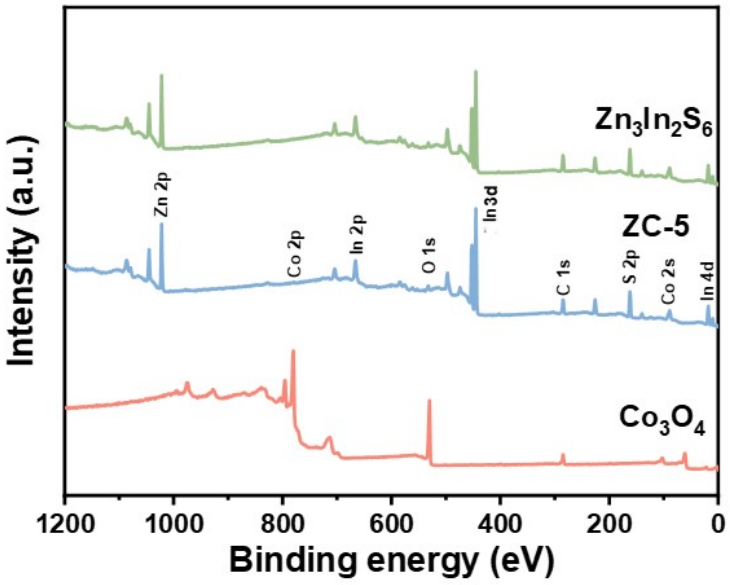

Fig. S3 XPS survey spectra of Co_3O_4, $Zn_3In_2S_6$, and ZC-5.

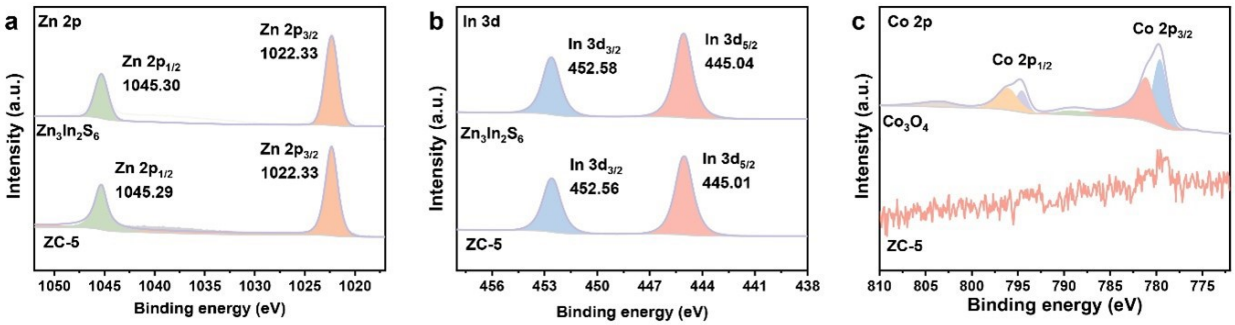

Fig. S4 High-resolution XPS spectra of (a) Zn 2p, (b) In 3d and (c) Co 2p.

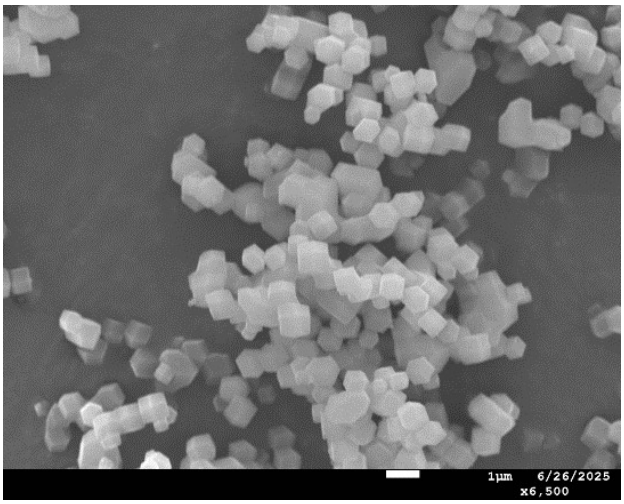

Fig. S5 SEM image of ZIF-67.

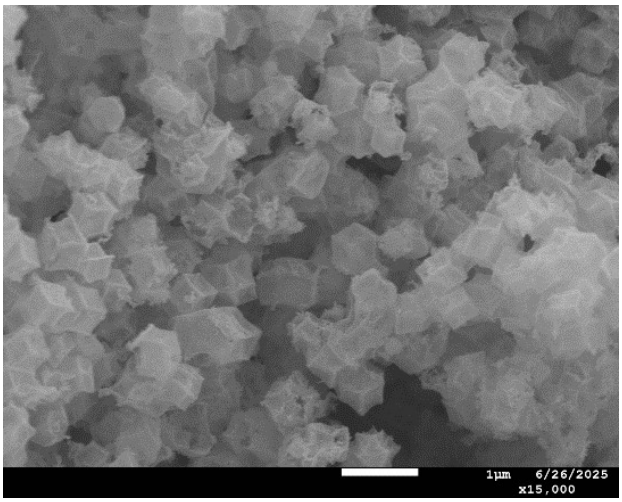

Fig. S6 SEM image of Co_3O_4.

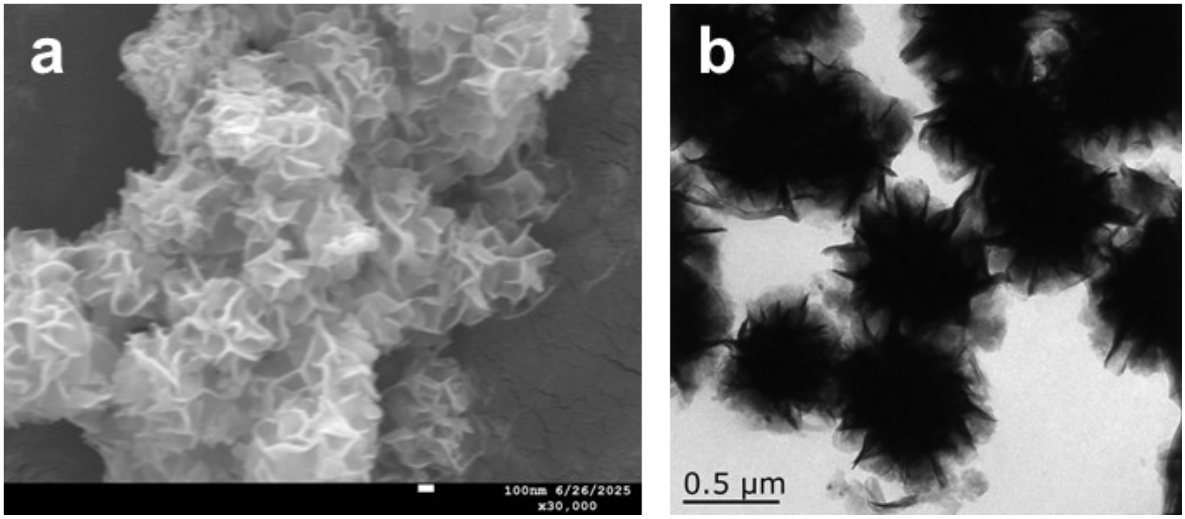

Fig. S7 (a) SEM and (b)TEM images of $Zn_3In_2S_6$.

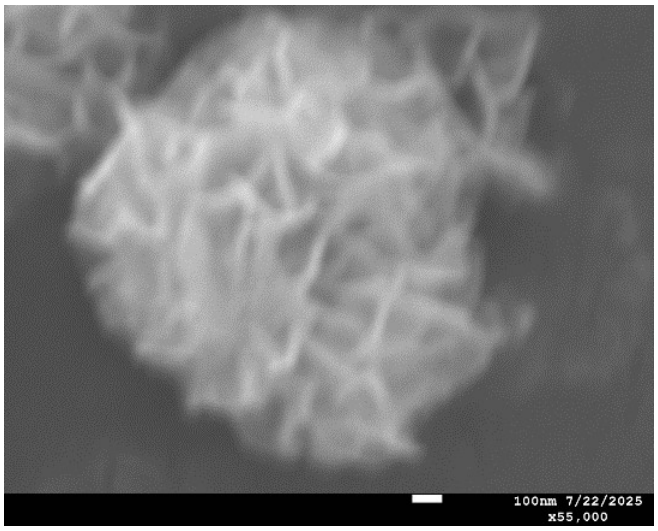

Fig. S8 SEM image of ZC-5.

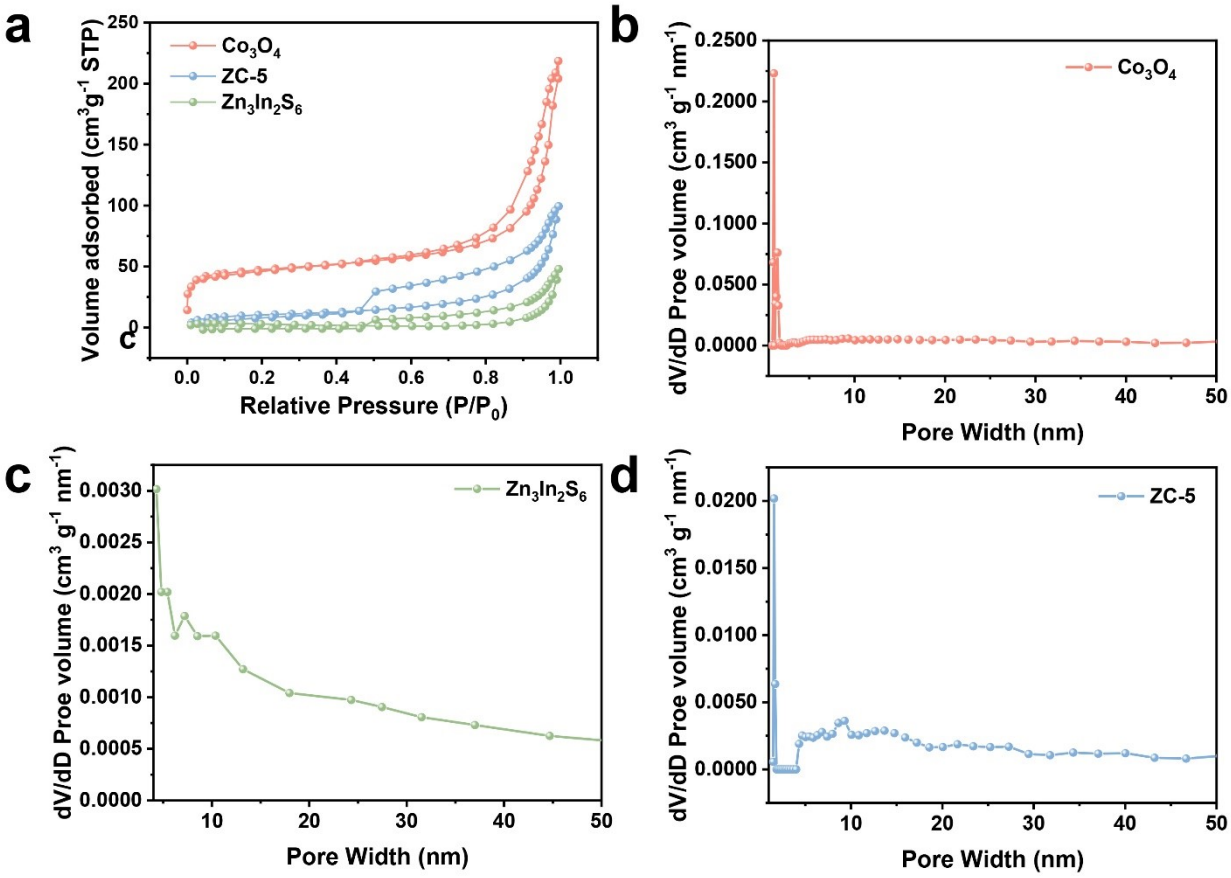

Fig. S9 (a) N_2 absorption-desorption isotherms and related pore size distribution profiles of (b) Co_3O_4, (c) $Zn_3In_2S_6$, and (d) ZC-5, respectively.

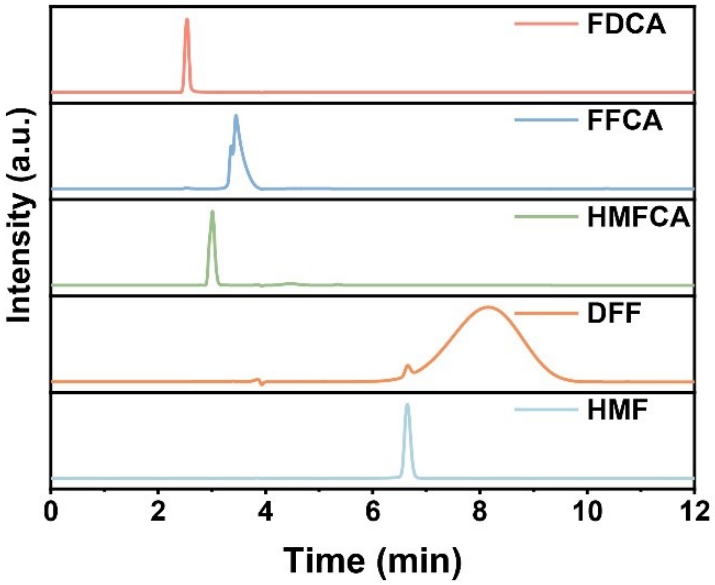

Fig. S10 HPLC spectra of HMF and different oxidation products.

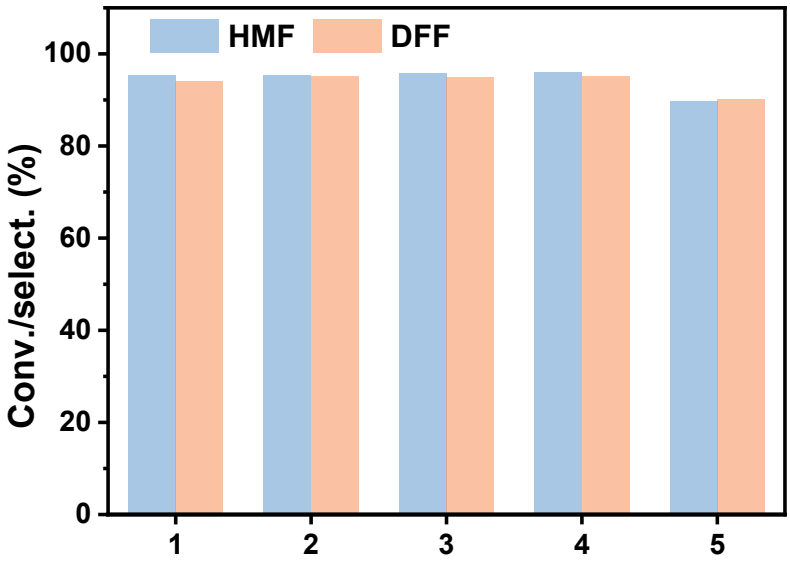

Fig. S11 Recycle test profiles of ZC-5.

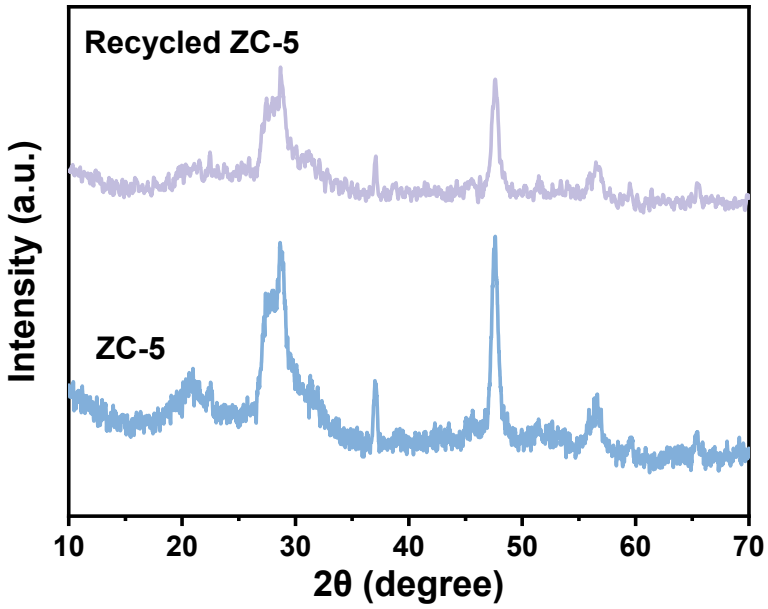

Fig. S12 Related XRD profiles of ZC-5 after recycle.

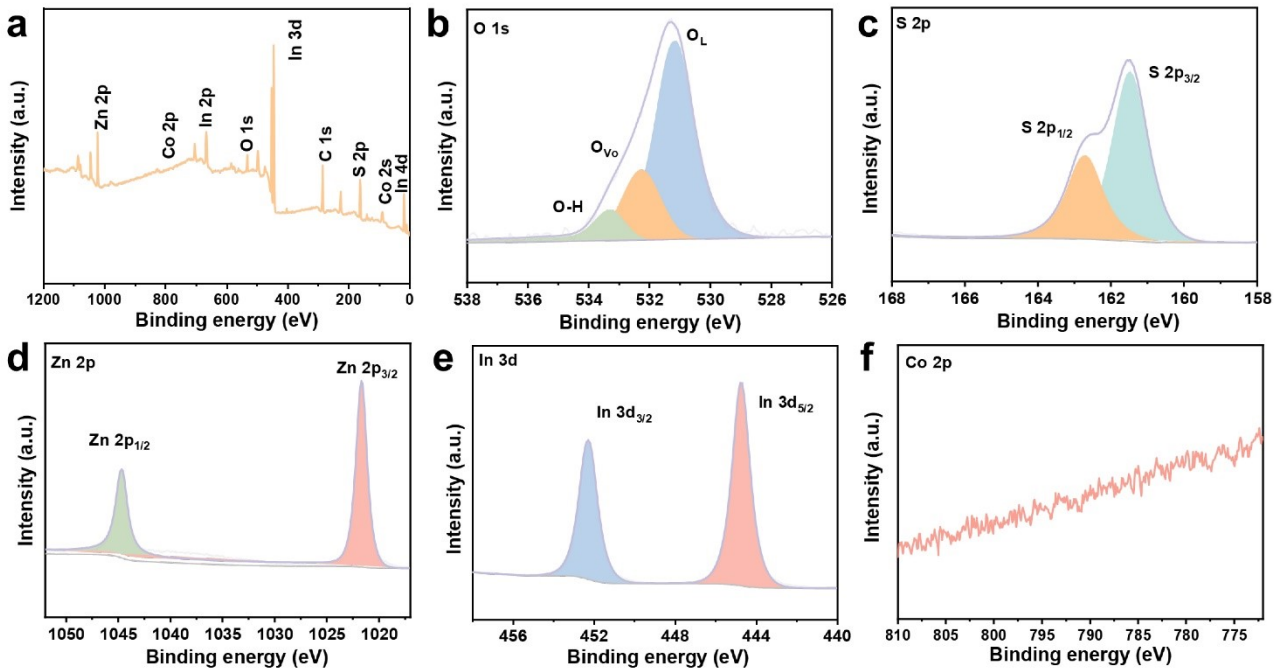

Fig. S13 XPS spectra of ZC-5 after recycle.

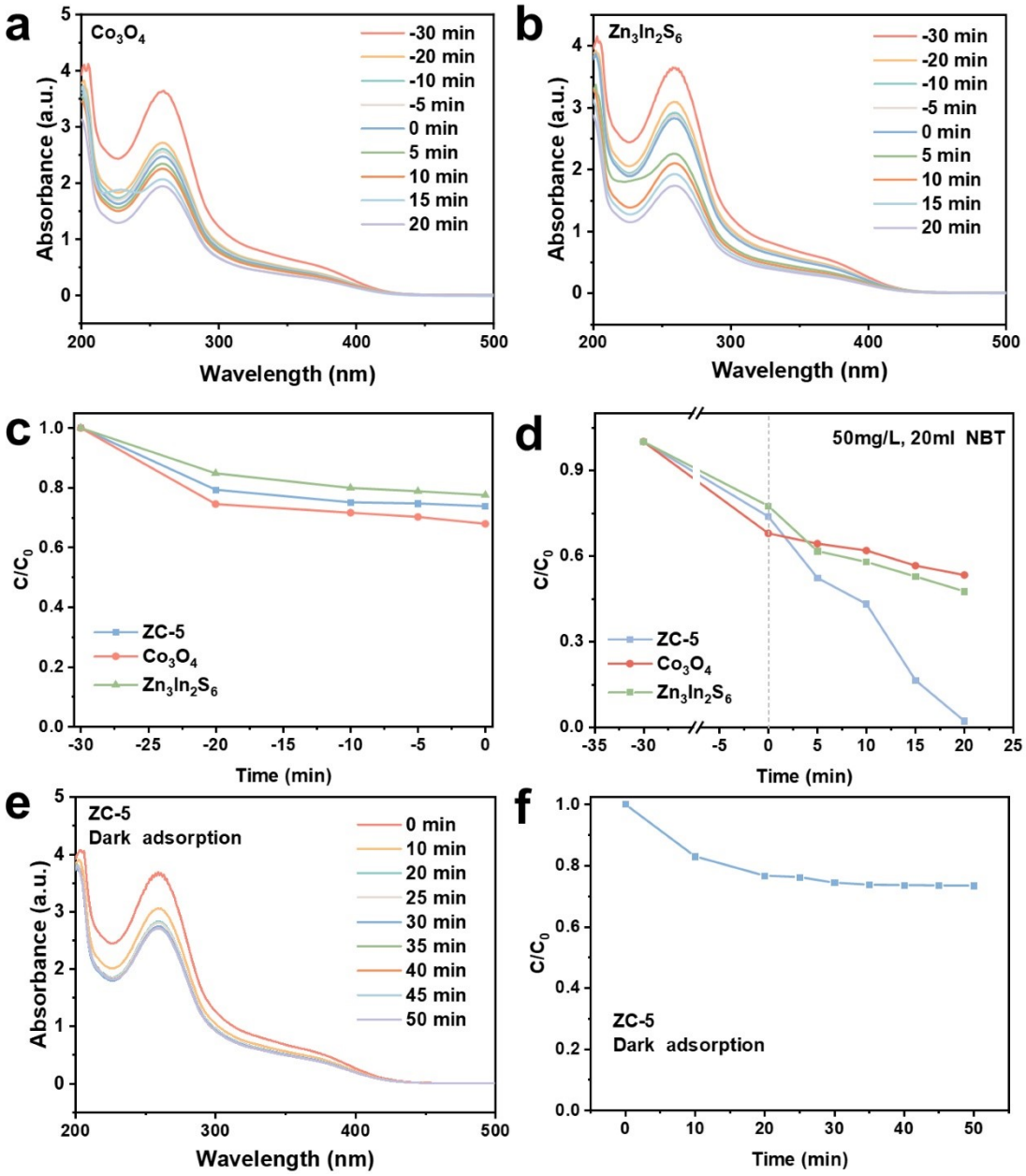

Fig. S14 UV-vis absorbance spectra of NBT degradation over (a) Co_3O_4 and (b) $Zn_3In_2S_6$. (c) Adsorption curve of Co_3O_4, $Zn_3In_2S_6$ and ZC-5 under dark. (d) NBT degradation activity curves of Co_3O_4, $Zn_3In_2S_6$ and ZC-5 under light irradiation. (e) UV-vis absorbance spectra and (f) adsorption curves of NBT over ZC-5 under dark.

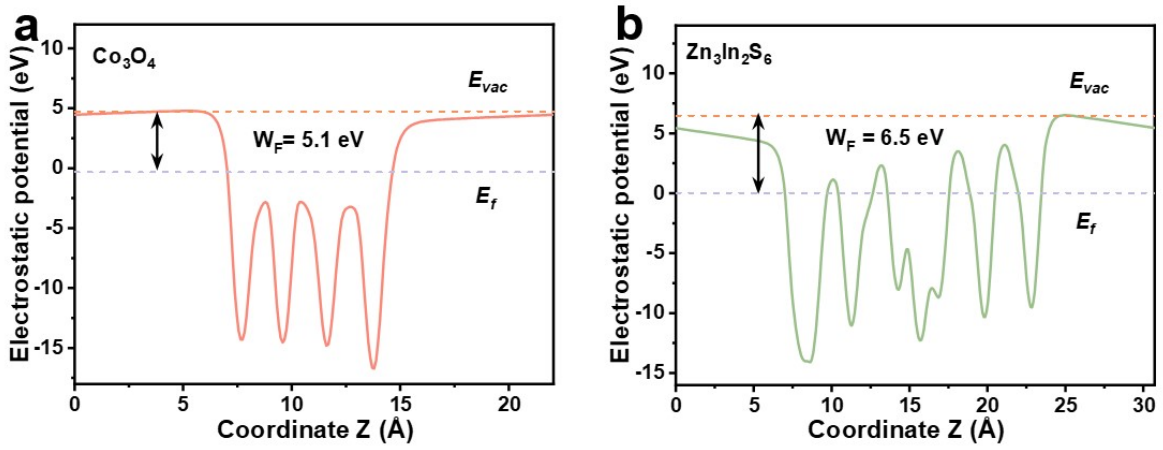

Fig. S15 Calculated work functions of (a) Co_3O_4 and (b) $Zn_3In_2S_6$.

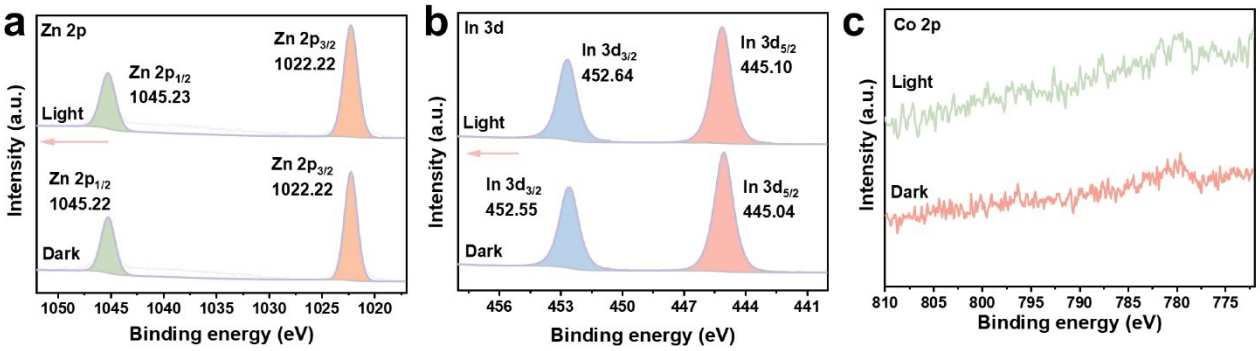

Fig. S16 In-situ XPS spectra of (a) Zn 2p, (b) In 3d, and (c) Co 2p for ZC-5 under light irradiation.

Table S1 Co_3O_4, $Zn_3In_2S_6$, and ZC-5.

Sample	S_{BET} ($m^2 \cdot g^{-1}$)	Pore volume ($cm^3 \cdot g^{-1}$)
Co_3O_4	176.2823	0.338041
$Zn_3In_2S_6$	13.6983	0.074129
ZC-5	38.7351	0.153726

Table S2 Lifetime parameters of $Zn_3In_2S_6$ and ZC-5 from the TRPL results.

Sample	τ_1 [ns]	A_1 [%]	τ_2 [ns]	A_2 [%]	τ_A [ns]
$Zn_3In_2S_6$	1.17	54.36	5.46	45.64	3.13
ZC-5	0.51	43.57	2.13	56.43	1.42

Table S3 Comparison of the results of HMF conversion by photocatalysis in water with other studies.

Entry	Catalyst	Light source	HMF Con. (%)	Reaction rate (mmol L^{-1} g^{-1} h^{-1})	DFF yield (%)	Time (h)	Ref.
1	TiO_2	black lamps (365nm)	50	0.5	13	16.3	3
2	TE-520-P25	15 W/10 Philips fluorescent lamps	50	1.3	17.5	4	4
3	Cu_2O/TiO_2	Xe Lamp (350-780 nm)	52	11.6	23	1.5	5
4	P-$Cd_{0.5}Zn_{0.5}S$	White LED (3 W)	40	-	26	8	6
5	Fe (III)/Bi_2MoO_6	500 W Xe lamp	32.62	1.6	31.1	-	7
6	$V_2O_5 \cdot nH_2O$/g-C_3N_4	visible light	42.5	0.2	35.7	4	8
7	$Cd_{1.5}In_2S_{4.5}$	500 W Xe lamp	68.8	181.8	43.2	6	9
8	$Zn_{0.5}Cd_{0.5}S/MnO_2$	30 W white LED bulbs	46.6	15.3	46.6	24	10
9	CTF-Th@SBA-	Blue LED	57.0	-	56.4	-	11
10	$Ti_3C_2F_x$ /$CdIn_2S_4$	500 W Xe lamp	78.5	32.7	60.3	12	12

11	$Sn_xIn_yS_{2x+1.5y}$	300 W Xe lamp	69.4	60.9	62.1	6	13
12	$ZnIn_2S_4/CuCo_2O_4$	445±10 nm LED light source (20 W)	88.6	33.2	63.0	4	14
13	ZIS/CuO	445±10 nm LED light source (20 W)	88.4	35.4	63.5	3	15
14	$ZnS/ZnIn_2S_4$	500 W Xe lamp	100	16.7	70.9	6	16
15	ZC-5	24 W LED light (450-465nm)	95.4	79.5	66.8	3	Ours work

References

1 J. Fan, L. Shi, H. Ge, J. Liu, X. Deng, Z. Li and Q. Liang, *Adv. Funct. Mater.*, 2024, **35**, 2412078.

2 T. Lu and F. Chen, *J. Comput. Chem.*, 2012, **33**, 580-592.

3 S. Yurdakal, B. S. Tek, O. Alagöz, V. Augugliaro, V. Loddo, G. Palmisano and L. Palmisano, *ACS Sustainable Chem. Eng.*, 2013, **1**, 456-461.

4 A. Akhundi, E. I. García-López, G. Marcì, A. Habibi-Yangjeh and L. Palmisano, *Res Chem. Intermed*, 2017, **43**, 5153-5168.

5 Q. Zhang, H. Zhang, B. Gu, Q. Tang, Q. Cao and W. Fang, *Appl. Catal. B*, 2023, **320**, 122006.

6 H.-F. Ye, R. Shi, X. Yang, W.-F. Fu and Y. Chen, *Appl. Catal. B*, 2018, **233**, 70-79.

7 J. Xue, C. Huang, Y. Zong, J. Gu, M. Wang and S. Ma, *Applied Organometallic Chem.*, 2019, **33**, e5187.

8 H. Wang, D. Huang, Q. Zhuge and Y. Wu, *Diam. Relat. Mater.*, 2023, **139**, 110413.

9 M. Zhang, Z. Yu, J. Xiong, R. Zhang, X. Liu and X. Lu, *Appl. Catal. B*, 2022, **300**, 120738.

10 S. Dhingra, T. Chhabra, V. Krishnan and C. M. Nagaraja, *ACS Appl. Energy Mater.*, 2020, **3**, 7138-7148.

11 C. Ayed, W. Huang, G. Kizilsavas, K. Landfester and K. A. I. Zhang, *ChemPhotoChem*, 2020, **4**, 571-576.

12 M. Zhang, Y. Zhang, L. Ye, Z. Yu, R. Liu, Y. Qiao, L. Sun, J. Cui and X. Lu, *Appl. Catal. B*, 2023, **330**, 122635.

13 S. Yu, C. Song, H. Zhang, W. Liao, D. Zhao, C. Len, H. Lü and T. Su, *J. Alloys Compd.*, 2024, **982**, 173810.

14 Y. Liu, W. Xue, J. Ye, R. Zhang, A. P. Rangappa and J. Zhao, *Small*, 2025, **21**, 2409005.

15 Y. Liu, W. Xue, J. Ye, R. Zhang, Y. Shao, A. P. Rangappa and J. Zhao, *Chem. Eng. J.*, 2025, **515**, 163620.

16 Y. Zhang, M. Zhang, Z. Yu, R. Liu, Y. Li, J. Xiong, Y. Qiao, R. Zhang and X. Lu, *Appl. Catal. B*, 2024, **350**, 123914.